In-Flight Separation of Projectile Fragments

D.J. Morrissey and B.M. Sherrill

National Superconducting Cyclotron Laboratory,
Michigan State University, East Lansing, MI 48824, USA

Abstract. The in-flight or direct production of secondary beams of radioactive ions is discussed. Two reaction mechanisms, fragmentation and fission of a fast projectiles, have been shown to be very effective at producing beams of an extremely broad range of interesting nuclei. The resulting nuclei have large forward momenta with relatively sharp angular distributions peaked close to zero degrees. Such narrow distributions are readily collected and purified with magnetic devices by exploiting atomic energy-loss processes in profiled energy degraders. With large aperture magnets and high energy primary beams, collection of nearly the full momentum and angular distribution of a given fragment are now possible, although the beam emittance may be poor and depends on the production mechanism. The features of the production reaction mechanisms, separation techniques, and a survey of the present and proposed devices are presented.

1 Introduction

Intense beams of a broad range of the most exotic nuclei are now routinely produced in laboratories around the world for decay studies, but more-so to induce secondary nuclear reactions. The technique that is the workhorse for making high-energy radioactive nuclear beams (RNB) relies on the kinematic (forward) focusing that present in certain peripheral nuclear reactions that occur with heavy projectiles at relatively high incident energies. The emergent exotic ions can be rapidly separated by in-flight techniques before they decay or come to rest in matter. This technique is usually called the "projectile fragmentation technique" but more correctly should be referred to as "in-flight separation" since a variety of reaction mechanisms besides projectile-fragmentation have been used to produce the nuclei. We will present a review of the production, separation techniques, beam properties and the recent ideas for collecting and thermalizing fast exotic beams.

Projectile fragmentation is a process through which very high energy (kinetic energy/nucleon $\sim m_0c^2$) nuclei are broken into smaller residues that retain most of the vector momentum of the beam. This process was originally studied in the 1970's at the BEVALAC accelerator. Nuclear physics experiments to produce exotic nuclei and to calibrate cosmic ray instruments using techniques centered on magnetic rigidity were pioneered with beam line elements at the Lawrence Berkeley Laboratory (LBL) [1]. Another group at LBL developed techniques to produce radioactive ^{11}C ions from a primary ^{12}C beam in which as much as 1%

of the incident beam was converted into ^{11}C ions and separated for implantation in biomedical samples [2,3].

The beam of exotic nuclei must be separated from the primary beam and from the other reaction products by some combination of magnetic and perhaps electrostatic elements acting on the distribution of ions. The initial work at LBL was dramatically extended when a degrader was placed in the middle of the LISE spectrometer at GANIL [4,5]. Selection according to magnetic rigidity alone gives a set of isotopes with a single momentum-to-charge ratio; passing this set of preselected fragments through a degrader breaks the redundancy because the momentum of each type of fragment is systematically shifted by the energy-loss process.

The primary beam passes through the production target and retains a large fraction ($\sim$90% or more) of its initial kinetic energy. Therefore, an advantage of in-flight separation techniques is that beams can be produced and delivered at high energy without the need for reacceleration. The process can be extremely efficient and the production target only needs to be able to dissipate a fraction of the beam power. The unreacted beam is collected at some other point in the separator itself. Radiation shielding is straightforward since the volume of the reaction chamber can be kept relatively small and the return yokes of the magnets provide local shielding. However, the radiation damage of nearby material and of the focussing and bending magnets is a serious concern and all elements of the production area must be made to function in a high radiation environment. The particle identification of fast ions is also relatively simple, and the contaminant level can be easily checked on-line.

A distinct advantage of the fast-ion achromatic devices (devices where the final position and angle do not depend on momentum) is that the purity of the secondary beams can be improved by passing the ions through profiled energy degraders at an intermediate dispersive point [6,7]. This can, in most cases, eliminate mass-to-charge ambiguities and provide essentially pure secondary beams for even the heaviest elements.

One final significant feature of in-flight separation is that the process is not sensitive to chemical properties or, in general, to the half-life of the isotopes of interest. The limitation on the half-life is only given by the flight time of the ions through the device, which is almost always less than one microsecond but longer, of course, in cooler rings. The net result is that, given suitable ion optics, the efficiency of the in-flight separation techniques can reach essentially 100%.

In-flight separation is not only a very useful and selective technique, but also one that is very sensitive. It has been shown at various laboratories that experiments can be performed where the production rate of a desired species is several per week as in the cases of ^{48}Ni [8] and ^{100}Sn [9,10]. Primary beam intensities of one particle-μA or $6x10^{12}$ ions/s are routine. Hence, the one atom/week level corresponds to a production cross section of $1x10^{-18}$ barns or 1 attobarn. That is an equivalent probability to detection of 1 atom produced per nearly 10^{18} collisions between beam and target.

The in-flight technique spawned many large facilities that were very productive during the last decade, the A1200 separator at the NSCL in the USA [11], the RIPS separator at RIKEN in Japan [12], the FRS device at GSI in Germany [13], the COMBAS separator at Dubna in Russia [14], and the upgraded LISE-3 system at GANIL in France [15]. The technique also is integral to the large facilities for the next decade, for example, the A1900 in operation at the NSCL [16], the Big-RIPS project under construction in Japan [17], and the Super-FRS recently approved for construction in Germany [18]. The most recent plan for the next major nuclear physics facility in the USA is a large exotic beam facility called "RIA" for rare isotope accelerator, that will incorporate two state of the art two-stage fragment separators. [19] These facilities use achromatic magnetic devices where "achromatic" means that the position and angle of ion at the end of the device (called the focal plane) do not depend on the ion's momentum. Such achromatic magnetic devices are generally most useful for efficient separation at higher energies because they can collect a large fraction of all the produced fragments and focus them to a small spot. An early paper by Schmidt *et al* [6] outlines the fundamentals of the use of achromatic devices.

Electric fields, although desirable because they can provide velocity (kinetic energy) separation, are generally not used by themselves at the higher energies characteristic of fragmentation reactions. The attainable electric fields can not sufficiently bend high rigidity fragments. However, Wien filters are used to improve the purity of RNB's. The upgrade of the LISE separator to LISE3 included a high electric field Wien filter to make a velocity separation of fragments separated by the LISE spectrometer [15]. A similar technique has been used at the NSCL in which the RPMS is used [20]. The range over which this additional separation is still practical ends around ∼200 MeV/nucleon.

As an illustration of the reach of the technique and the ions that will be available at the next generation of in-flight separation facilities (such as RIA, RIKEN, and GSI), Fig. 1 illustrates the expected radioactive ion (rare isotope) beam intensities based on projectile fragmentation cross sections and a 10% momentum acceptance fragment separator. The beam power is assumed to be 100 kW and the primary beam energy is 400 MeV/nucleon. The production target is adjusted to fill the separator momentum acceptance. The primary beam is optimized for each fragment, i.e., the best stable beam is chosen for each secondary fragment. The production cross sections are taken from the EPAX2 parameterization [21], discussed below. The figure is not intended to be correct in all details and reality may be very different depending on the production cross sections very far from stability. The proton-rich rp-process nuclei will be produced in relatively large quantities and it is exciting to think about experiments with a significant number of neutron-rich r-process nuclei that will be available. At the limits of stability, it may be possible to reach the drip line for nuclei as heavy as ^{120}Zr. However, as is clear in the figure, these most interesting nuclei are produced at very low yields and it will remain a challenge to perform experiments with a very small number of nuclei.

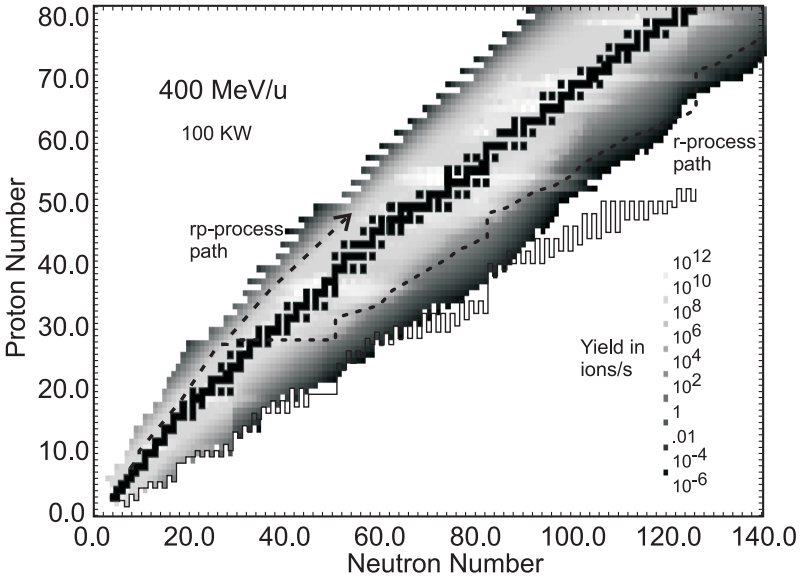

Fig. 1. Intensities for in-flight separated secondary beams produced by projectile fragmentation from a 100 kW 400 MeV/nucleon primary beam as described in the text. The region of known nuclei is outlined with the solid line and the approximate path of the rp-process and the r-process are indicated by grey lines.

Several review articles are available on aspects of the in-flight separation technique [22–25] and it is important to recognize that this technique is not limited to high beam energies. Here we discuss the general features of the reaction mechanisms that have been used to produce radioactive beams by in-flight in section 2 with a short discussion of so-called recoil separators. In section 3 we review the separation techniques used to purify the secondary beams. Some discussion is given on the possibilities for expansion of the techniques in new facilities and we discuss experimental techniques that can be used to overcome some of the problems associated with the poor emittance of these RNB's. In section 4 we consider the recent advances in the collection and thermalization of RNBs. Finally in section 5 we offer some conclusions and an outlook.

2 Useful Nuclear Reaction Mechanisms

2.1 Projectile Fragmentation

Projectile fragmentation was first described in reactions of heavy ions with kinetic energies on the order of 200 MeV/nucleon or more [31,32]. The general features of the reaction mechanism seem to remain the same at energies as low as 50 MeV/nucleon but clearly change by ∼10 MeV/nucleon. In a nutshell, the process involves a peripheral interaction of the projectile with a target nucleus

in which some nucleons are removed and the excited residue undergoes a small recoil from the removal and an isotropic recoil from the de-excitation. Coulomb deflection and the nuclear recoil of the ion are small so that the large initial velocity can focus all the products into a narrow cone. The mass, charge, and velocity distributions of the residues have been equally well described in microscopic nucleon-nucleon scattering models or macroscopic abrasion framework partly because all the models predict the creation of excited primary residues that must undergo statistical de-excitation [33].

The intranuclear cascade model of proton-induced reactions was generalized to nucleus-nucleus collisions by Yariv and Fraenkel [34,35]. This model relies on assumptions that are valid in the region of 0.1 to 1 GeV/nucleon and the calculation traces the nucleon-nucleon scattering of the overlapping particles initially bound in the target and projectile. The computer model (ISABEL) gives somewhat narrow distributions of target and projectile residues that have very high excitation energies. A statistical de-excitation calculation is used to predict the observed ground-state nuclei. Fauerbach has coupled the ISABEL code to a modern statistical de-excitation code written called PACE and the predicted isotopic cross sections from the resulting program (ISAPACE) are remarkably good [36].

On the other hand, a macroscopic model based on the removal of nucleons in the volume eclipsed by the target and projectile and the subsequent de-excitation of the primary products also has been successful [37,38]. This approach is called alternatively the participant-spectator model or more commonly the abrasion-ablation model. The target nucleus is imagined to shear off part of the projectile, leaving the rest of the projectile to travel forward at the initial beam velocity, with a minor down-shift in velocity and some excitation energy. The primary residues (projectile or target) then undergo statistical de-excitation processes leading to the observed products [39]. This model has been extended in terms of a more microscopic calculation of the excitation energy and the angular momentum of the residues by Schmidt and coworkers [40,41].

A remarkable feature of the observed fragment cross sections is that they are relatively constant from approximately 40 MeV/nucleon to 2 GeV/nucleon with the exception of the fragments whose mass number is lower than, but still close to that of the initial nucleus [42,43]. The cross sections are largest for fragments close in mass, but lower, than the initial nucleus and decrease exponentially with decreasing mass number. The isotopic distributions are nearly Gaussian and have a most-probable neutron number that is significantly lower than that for stability. The near constancy of the production cross sections allows simple empirical parameterizations of the existing cross section data to make quite good estimates. For example, a generalized parameterization [44] of proton-induced reaction data originally by Rudstam [45] was able to predict essentially projectile and target fragmentation cross sections. The parameters were fitted to data taken from a wide range of target and projectile fragmentation studies and the overall agreement with many measurements is quite good. The parameterization is expected to be valid at high energy in which the cross sections become constant

but a number of results measured at GANIL, MSU and RIKEN with beam energies in the range of 50 to 100 MeV/nucleon also agree with the predictions. The initial estimates of cross sections needed to plan experiments are usually made with this parameterization and only minor modifications have been made in a revised parameterization [21].

The production cross-section of a given projectile residue depends on the target through a geometrical factor in the high energy limit of fragmentation reactions and only fragments that are lower in mass than the projectile are expected to be produced. However, nucleon transfer can be seen to play an important role at lower beam energies. First, a strong target dependence is observed for the *yields* of nuclei far from stability. Very neutron-rich nuclei are best produced with heavy production targets and proton-rich nuclei near the limit of stability are produced with the heavier N$\sim$Z targets. A few nuclei with atomic numbers greater than that of the beam were also observed but the mass number is generally lower than that of the beam. Thus, charge exchange reactions or even Delta-formation (at high energies) may take place leaving the residue with a large amount of excitation energy. On the other hand, neutron pickup products have also been observed in 80 MeV/nucleon ^{18}O reactions on ^{9}Be and ^{181}Ta targets [46] indicating that some cross section is still present for few nucleon pickup at modest bombarding energies. The nucleon pick-up products provide special insight into the reaction process, see below.

In addition to the production cross section, the other key ingredient of the projectile fragmentation mechanism that determines the brightness of the secondary radioactive beam is the fragment momentum distributions. The momentum distributions directly determine the parallel (or longitudinal) emittance of the fragment beams. The emittance is the volume of phase space that contains all coordinated of particles in the beam. The longitudinal emittance refers to the projection of the phase space on the momentum-time axes. The transverse emittance (or perpendicular emittance) referees to the projection on the geometric axes of position and angle in the horizontal and vertical planes. Emittance is discussed further in section 3.3, but depends primarily on the recoil momentum distributions of the fragments. The momentum distributions are characterized by a small down-shift in velocity and a nearly Gaussian spreading that is larger than the down-shift. In a very early study, Goldhaber [48] showed that the momentum width of fragment created in a direct breakup process is related to the Fermi momentum of the removed nucleons. For the momentum parallel to that of the beam, one writes:

$$\sigma_{\parallel}[MeV/c] = \sigma_0 * \sqrt{\frac{A_f(A_b - A_f)}{A_b - 1}} \tag{1}$$

where σ_0 is a fraction of the mean Fermi momentum of the removed nucleons, A_b and A_f are the number of nucleons in the beam and fragment, respectively. The theoretical value of σ_0 should be approximately 100 MeV/c based on electron scattering measurements but the experimental data is better described by the smaller value of 85 MeV/c (for beam energies $\geq$40 MeV/nucleon), on the order

of 80 to 90% of the Fermi momentum. This difference has been explained as an effect of the Pauli principle which limits the number of nucleons which can participate [49], although the predicted target dependence of this explanation has not been reported. The large role that statistical excitation in these reactions also directly contributes to the growth of the variance of the parallel momentum with the mass loss $(A_b - A_f)$ [50].

The parallel and perpendicular momentum distributions should be the same if nuclear and Coulomb scattering make small contributions to the deflection, that is, at high beam energies. At bombarding energies from 30 to 200 MeV/nucleon this description is apparently also valid, although the reaction mechanisms may not be simple. An important difference at low energies is that an orbital dispersion is present that adds a contribution to the perpendicular momentum width $\sigma_\perp$ according to the expression:

$$\sigma_\perp[MeV/c] = \sqrt{\sigma_\parallel^2 + \sigma_N^2} \tag{2}$$

where σ_N was found to be approximately 200 MeV/c. [51,52]

Another important feature is that the momentum distributions are not fully Gaussian at low energies, and develop a low energy tail due to dissipative effects in the reaction. This low energy tail can contribute significant background to secondary beams that separated by strictly magnetic analysis. An example of the broad range of fragments that are can be observed in a single setting of a separator is shown in Fig. 2 from the work of Pfaff et al. [47]. All of the isotopes shown in this figure fell within ±1.5 percent of the central momentum and thus passed through the A1200 separator (no profiled degrader was used, see discussion below).

Another interesting and potentially very useful feature of these reactions is that the nuclear spin of fragments produced at finite angles can be polarized and the polarization can be maintained through the analysis system. The polarization arises from the localization of the impact at the periphery of the nucleus and should be linked to the linear (parallel) momentum distribution. Asahi and coworkers showed that up to 20% of the ^{12}B fragments observed at 5 degrees from a 40 MeV/nucleon ^{14}N beam were polarized [53]. Further, the amount and direction of the polarization was found to be correlated with the fragment momentum. The systematic behavior of the polarization of the spin continues to be studied [54]. The polarization of nuclei formed by a proton pick-up reaction, ^{37}K from ^{36}Ar, was found to be large and positive at the peak of the yield distribution [55]. These important new results confirm the picture that the nucleon picked up from the target has an average linear momentum equal to the Fermi momentum aligned with the beam direction, as was suggested by earlier observations of the linear momentum distributions of neutron pick-up products [46]. The large polarization at the peak yield may provide an important new tool to study nuclear magnetic moments.

Although a considerable amount is known about peripheral reactions in the 50 MeV/nucleon to 2 GeV/nucleon range, there are still important aspects about the reaction mechanism to study. Treatments of the reaction tend to include the

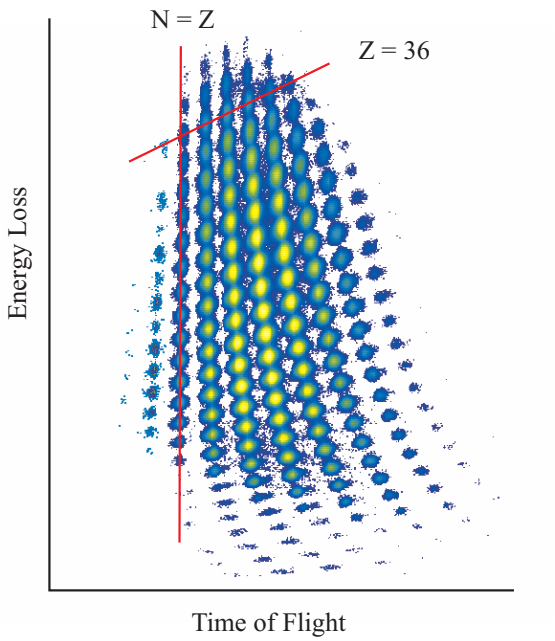

Fig. 2. The projectile fragments observed in one setting of the magnetic rigidity in the A1200 separator from the reaction of ^{78}Kr wtih ^{9}Be at 70 MeV/nucleon [47] are shown as a function of energy-loss and time-of-flight. The vertical line indicates the position of nuclei with N=Z and the diagonal line indicates the positions of krypton isotopes.

target only through a geometric factor but the recent studies of uranium, lead, and gold reactions by Schmidt et al. [56] show a dramatic target dependence for light targets. Another important question for the production of nuclei very far from stability is whether these simple descriptions are valid for nuclei produced at the limits of stability. For example, the "fragile" nucleus ^{11}Li that has no bound excited state is produced at rates that are consistent with the systematics for production of (much) more stable nuclei. Presumably the fragile nuclei must be formed in relatively cold processes, yet the models predict that the fragmentation process is not, in general, cold. Other aspects of the reactions are not fully understood such as the role of dissipative and transfer processes below 200 MeV/nucleon and the reduction of σ_0 from the value consistent with the internal Fermi momentum.

2.2 Projectile Fission

Although projectile fragmentation is used to produce light neutron-rich nuclei, the maximum yield of projectile fragmentation products is obtained for neutron-deficient nuclei. On the other hand, nuclear fission has been an extremely important source of neutron-rich nuclei for a long time. The fission process creates

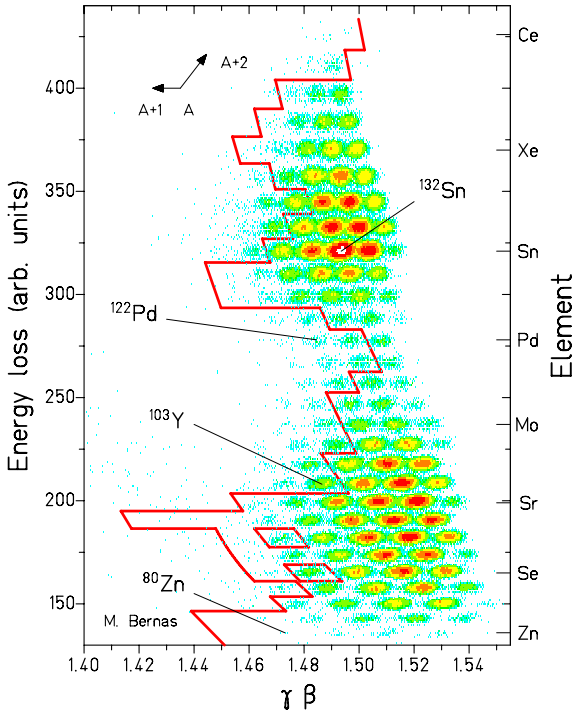

Fig. 3. The yields of nuclei from the fission of ^{238}U determined by Bernas et al. [29] are shown as a function of velocity ($\gamma\beta$) and energy loss which are equivalent to mass and atomic number, respectively. The jagged line indicates the boundary between nuclei that had been previously observed (right side) and those observed for the first time in that work (left side).

nuclei with a kinetic energy of approximately one MeV/nucleon in the rest frame of the fissioning nucleus and the angular distribution of products is essentially isotropic for low values of angular momentum. Thus, the recoil vectors of the products are distributed on the surface of a slightly diffuse sphere. When the fissioning nucleus is moving with a kinetic energy that is large compared to the fission recoil then the products can be collected and separated using in-flight techniques similar to those used for projectile fragments. However, generally only one or the other kinematic solution, e.g., forward-going or backward-going in the rest frame, can be accepted by present separators. Even with this limitation the fission of very energetic projectiles is an important process for the production

of neutron-rich nuclei due to the lack of other methods to produce these nuclei. A dramatic demonstration of the range of exotic nuclei produced in projectile fission can be seen in Fig. 3 from Bernas et al. [29].

2.3 Nuclear Fusion

A general feature of nuclear fusion reactions is that the products have linear momenta that are significantly lower than that of the beam. The momentum is larger than that of the target, of course, and the fusion products are said to recoil out of the target. Many recoil collection devices have been designed for near coulomb-barrier energies. Recoil separators often employ electric fields to cancel the velocity dispersion created by a magnetic separation leaving only a dispersion in the mass-to-charge ratio [20,26,27]. A detailed discussion of this technique also has been given by Wollnik [28] and a discussion of the application of recoil separators is presented in this volume by Julin and by Woods.

The beams from these recoil separators suffer from some contamination since the separation technique is only sensitive to the atomic *mass-to-charge* ratio of the ion and not strictly the nuclear *mass-to-proton number* ratio of the ion. In addition, different charges states of a given isotope will be separated from one another giving a lower overall collection efficiency. A solution to remove the mass-to-charge ambiguity and improve efficiency is to use the gas-filled separator technique [30] in which the spectrograph is filled with a few mbar of buffer gas. The moving ions reach an equilibrium charge state that is proportional to the ion's velocity. Thus, each ion will have a unique mass-to-average-charge (with some spread) so that the final position is just determined by the mass of the ion. So far this technique has not been applied to produce secondary beams of rare ions for further reaction.

2.4 Target Considerations

The influence of the target material on the fragment yields comes from the interplay of the nuclear cross section and the perturbation of the beam properties by electronic interactions (energy loss and multiple scattering). Geometrical models of the reaction cross section have been very successful up to this point so that low-Z target materials are preferred. The overall production rate is larger with low-Z materials due to a larger number of atoms for a given number of electrons. Beryllium and to a lesser extent graphite (carbon) targets are used at existing fragmentation facilities.

The ion optics of fragment separators (discussed below) require that the width of the beam spot on-target be approximately less than 1-mm to allow high selectivity in the separation and purification of the secondary beams. The resolving power of the device is inversely proportional to the beam spot size. The beam spot size also enters directly into the transverse emittance (see section 3.3). Therefore, the beam energy is delivered to a target volume on the order of a few cubic millimeters. Dissipation of the thermal heat delivered to fragmentation targets in such small volumes has become an important problem. The dissipated

beam power can be estimated because the production of a given fragment has an optimal beam and target thickness. Note that in order to be collected the momenta of an isotope produced at the beginning and at the end of the target have to fall within the acceptance of the separator. The differential energy loss between the beam nucleus and the isotope to be collected thus determines the optimal target thickness for a given separator and the energy lost in the target by the beam. Typically the percentage of beam energy lost in the target by the beam is similar to the percentage momentum acceptance of the separator. An example of a difficult case, the yield of ^{38}Ca fragments from a 140 MeV/u ^{40}Ca beam in the NSCL-A1900 separator is optimal from a ∼700 mb/cm^2 beryllium target. Each calcium ion would deposit ∼37 MeV/u or ∼1500 MeV in the target which is 1.5 kW per particle-μA of beam current. Thick (∼mm) foils of these materials can absorb up to a hundred watts or so of beam power with moderate provisions for cooling so that the beam current and overall yield will be limited by target heating. The higher-Z beams at facilities under construction in Japan (RIKEN), in Germany (GSI), and proposed in the USA (RIA) will require new target designs to operate at the rated beam currents.

Advanced designs for cooling targets have included a rapidly rotating graphite wheel in operation from some time at GANIL [57] and new designs of similar systems for the big-RIPS [17] and for the super-FRS [18] separators. Nolen has pointed out that liquid lithium is another choice for target material partly because it is also an excellent cooling medium. [58] Since the density of beryllium is about four times that of lithium, the combination of beryllium metal with liquid lithium cooling could be used to provide a contained target system. The most powerful beams available at the NSCL are in the mass range between oxygen and calcium where beam powers range up to 4.5 kW. Target thickness in the range from 0.7 to 3 g/cm^2 are optimal for the acceptance of the A1900 separator and a first-generation target of this type is currently under construction [58]. Thick, windowless liquid-lithium targets are being studied for use with high intensity uranium beams at the proposed, next-generation radioactive beam facilities. Targets for the in-flight separators have yet to be developed that will sustain the power density created by the proposed (400 kW) uranium beams at RIA. The general safety issues associated with liquid alkalis have been explored in fusion research programs and for liquid-metal cooled reactors. The NSCL beryllium-lithium target will use a closed lithium loop and can be viewed as an intermediate step towards the operation of a windowless projectile fragmentation target.

3 In-flight Separation with Profiled Degraders

3.1 General Characteristics

One of the largest difficulties of beams produced by projectile fragmentation is that the secondary beam emittance is unavoidably large due to the random recoil momentum of the fragment created by the nuclear reaction. This emittance shrinks with increasing beam velocity. None the less, the resulting energy and

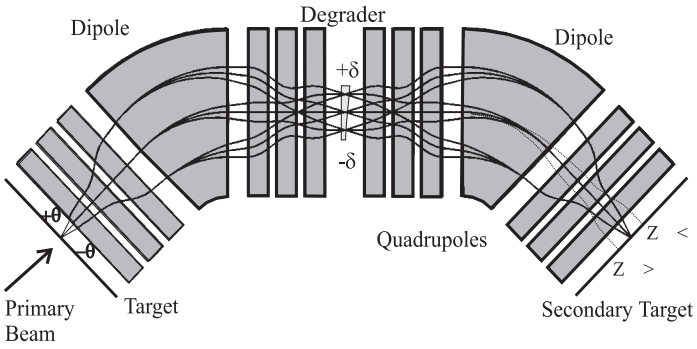

Fig. 4. Schematic representation of the ion-optics used in a momentum-loss achromat to separate projectile fragments.

angular spreads of the RNB's are much larger than those of a standard beam from an accelerator (by a factor of ten or more). In fact, the total emittance of secondary beams is determined by the combination of the nuclear reaction kinematics and atomic processes such as multiple angular scattering and energy loss straggling in the production target and in any degrader. We will outline the use of *profiled* degraders that can reduce the emittance, for example an achromatic degrader reduces the emittance by a factor of four [6]. The RNB kinetic energy spread is also relatively large, i.e. on the order of several percent, this quantity directly depending on the momentum acceptance of the separator. The kinetic energy distribution can be measured via the flight time of the ions to the secondary target and corrected on a event-by-event basis. Alternatively, a *monokinetic* degrader can be used from which all the ions will emerge with the same energy. A review of degrader shapes, uses and effects has been published by Geissel [7].

The highest resolving power for the various fragments is obtained if the system is achromatic. The term *achromatic* is used in practice to mean that the horizontal position and angle of a particle at the end of the separator does not depend on its momentum. Achromatic systems have the advantage that the final spot size is kept small even when the momentum acceptance is large. Fig. 4 illustrates the basic ion-optical concepts of fragment separation in a momentum-loss achromat with one stage of filtering. The ion trajectories for different momenta and initial scattering angles of the same isotope are indicated by the lines in the figure. Note that the ions are focussed to a small spot at the final focal plane of the device, independent of the initial angle or momentum. The key elements in the device are an initial bend for momentum-to-charge ratio selection and beam rejection, an energy loss degrader for atomic number separation also called a 'wedge', and a second bend for momentum-to-charge ratio selection of a specific ion. (We will assume that all the ions are fully stripped for the moment.)

The angular acceptance can be set by an aperture after the target or simply by the quadrupole magnets themselves at the beginning of the device. The

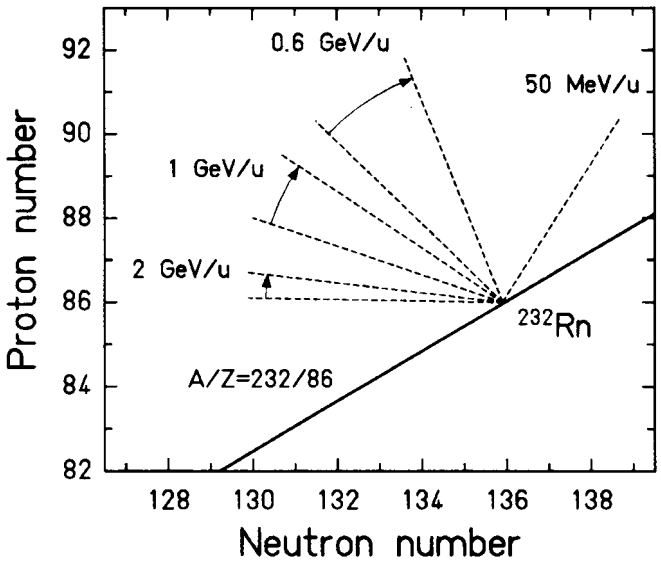

Fig. 5. Illustration of the directions of the two selections made in a momentum loss achromat in the N-Z plane, taken from Schmidt, et al. [6] The solid line represents the effect of the first bend that selects according to Bρ or approximately A/Z. The second selection, represented by the dashed lines, is determined by the Bρ *change* of each ion on passing though the degrader. The second selection is thus velocity dependent. The dashed lines were obtained by varying the thickness of the degrader from 0% to 80% of the ion's range.

momentum acceptance of the device is generally limited by the magnet bores or by an aperture at the intermediate position. Since the fragmentation nuclei are produced at nearly the same velocity, the initial Bρ=p/q or momentum-to-charge-ratio selection is essentially a mass-to-charge-ratio separation. Even so, projectile fragmentation reactions can produce many different ions that have the same mass-to-charge ratio, e.g. the fragmentation of an ^{18}O beam will produce five ions with m/q=3: ^{3}H, ^{6}He, ^{9}Li, ^{12}Be, and ^{15}B. An energy degrader can be inserted into the beam at the intermediate momentum-dispersive image to break the ambiguity among the ions that have the same initial mass-to-charge ratio because the energy lost in the material will depend on MZ^2/E or $(Z/v)^2$. The momentum lost will be approximately proportional to (Z/v). Again, because the ions have approximately the same velocity they will lose different momenta in the degrader depending on their atomic number and will exit the foil with different magnetic rigidities. The contaminants can then be dispersed at the focal plane by an additional bend. This Z-dependent separation is proportional to the degrader thickness and to the ratio of the magnetic rigidity of the second half of the system to that of the first half. The effect of this selection procedure is shown schematically in Fig. 5, taken from Schmidt, *et al.* [6]. While the selection

in the first half is approximately constant, if we consider reactions at different beam energies, the second selection will occur with a velocity dependent slope. Note that when the fragment's kinetic energy per nucleon is just below 1 GeV/u the selection in the second half is approximately perpendicular to the selection in the first half; this condition provides isobaric selection. At lower energies per nucleon, the selection in the second half becomes an isotonic selection.

An example of the selection of fragments is shown in Fig. 6. The separation of ^{80}As ions from the fragmentation products of a 140 MeV/u ^{86}Kr beam with the A1900 separator using a narrow momentum selection (Δp/p=0.5%) were calculated with the LISE++ code [59]. The panels show the nuclidic intensities as they leave the target, pass the intermediate image, and reach the focal plane. The values of the rates for the selected isotope, ^{80}As, with a 315 mg/cm^2 beryllium target and a 346 mg/cm^2 aluminum achromatic wedge, as well as the purity and the acceptance of the ^{80}As beam, are given in Table 1.

The mass resolving power of a fragment separator can be expressed in first order as:

$$R_{mass} = \frac{(x/\delta)_1}{(x/x)_1 \cdot x_0} \cdot \frac{(\delta/\delta_m)}{(\delta/\delta_0)} \tag{3}$$

where $(x/\delta)_1$ is the dispersion of the first set of dipoles, $\delta = (p - p_0)/p_0$ is the percent momentum deviation from the central momentum, $\delta_m = \frac{(m-m_0)}{m_0}$ is the percent change in the momentum caused by a percent change in mass, A, at the degrader with the charge held constant, x_0 is the initial spot size, and $(x/x)_1$ is the magnification at the dispersive image. In each case the subscript *0* denotes the value for the central ray. A very similar expression can be written for the charge resolving power:

$$R_{charge} = \frac{(x/\delta)_1}{(x/x)_1 \cdot x_0} \cdot \frac{(\delta/\delta_z)}{(\delta/\delta_0)} \tag{4}$$

where $\delta_z = \frac{(z-z_0)}{z_0}$ is the percent change in the momentum caused by a percent change in the atomic number, Z, at the degrader with the mass and momentum held constant. Eqs.3 and 4 are valid for an achromatic system with the condition:

$$(x/\delta)_2 = -(x/x)_2 \cdot (x/\delta)_1 \tag{5}$$

in which the degrader is shaped to preserve the achromatism (achromatic degrader). The important point to notice is that the first term in both equations for the resolution is simply the momentum resolving power of the first half of the separator. Hence, lower momentum resolving power always implies less pure secondary beams. To obtain mass resolving powers on the order of 200, the intrinsic momentum resolving power of the device should be 1000 or greater. This requirement has important consequences for the design of the separator and indicates that the emittance of the primary beam should be as small as possible in order to reduce the spot size, x_0, and thus increase the resolving power. The emittance of the secondary beam is also determined by the initial beam spot size. We should note that, in general, it is not necessary to use degraders with

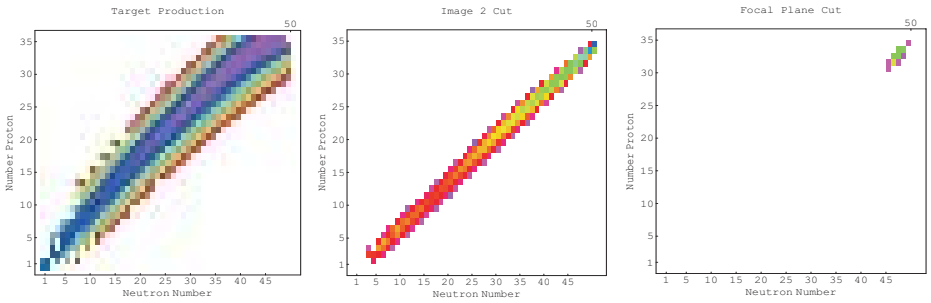

Fig. 6. Illustration of the results of the three selections made in a momentum loss achromat in the N-Z plane. Left-most panel: the production rate for fragments emerging from the target in the reaction ^{9}Be(^{86}Kr,^{80}As) at 140 MeV/A on a logarithmic scale in the range of 10^{-1} to 10+6. Center panel: the yields of fragments that survive a narrow B$\rho = \pm 0.5\%$ selection in the first half. Right-most panel: the yields of fragments that reach the focal plane.

achromatic profiles. An alternative approach is to use a "homogeneous" or flat degrader and tune the magnetic components of the second half to match the dispersion of the beam after the flat degrader.

The use of any degrader does increase the transverse emittance of the beam. As an illustration, if we assume both halves of a separator are identical and an achromatic wedge is placed at the center of the device (this is normally the case), then the increase in emittance is given by:

$$\epsilon = \epsilon_0 \times (1 - \frac{t}{R})^{-1} \tag{6}$$

where ϵ_0 is the initial initial emittance of the beam before the degrader and t is the thickness divided by the range, R, of the ion.

So far we have discussed the use of only one degrader within an ion optical system. There are several reasons to consider multiple stages of separation. The use of separation with two degrader stages has been discussed by Geissel *et al.* [18]. Two stages of separation reduce the contamination from secondary products

Table 1. Characteristics of a typical separation for the case of ^{9}Be(^{86}Kr,^{80}As)

	Target	Intermediate Image	Focal Plane
Rate†	1.1x10^{5}	5.6x10^{3}	1.1x10^{3}
Purity	0.00099	0.044	0.33
Acceptance	1	0.049	0.0099

†rate of ^{80}As in particles per second per particle-nA of primary beam, see text.

produced in the first wedge. Normally if many ions interact in the wedge, a large number of light products are produced and appear in the secondary beam. The other main advantage relates to the change in selection as a function of energy as shown in Fig. 5. The first selection occurs at a higher energy then the second selection due to energy loss in the first wedge so that the cuts have different angles in the A vs. Z plane. The second selection can eliminate many of the contaminant ions remaining after the first degrader selection.

3.2 Computer Simulation of In-flight Separation

Several programs exit to calculate the performance of in-flight separators and the expected yields. The most commonly used program is LISE [59]. LISE includes the parameters of the general configurations for most of the existing fragment and recoil separators. For a new design, a program such as TRANSPORT is used to calculate the first order beam optics and these parameters are input into LISE. More sophisticated programs that included higher order optics and secondary reactions are also available. The most readily available and reliable code of this type is MOCADI [60].

3.3 Transverse Beam Emittance

A major drawback to in-flight separation is the poor longitudinal and transverse beam emittance arising from the primary nuclear reaction, multiple scattering in the target and wedge, and the acceptance of the device. The transverse secondary beam emittance is approximately given by the expression:

$$\epsilon_0 = x_0 \times \Delta\theta \ [\mathrm{mm \cdot mr}] \tag{7}$$

where x_0 in the production target spot size, and the angular spread $\Delta\Theta$ is given by the maximum of the separator acceptance or by the nuclear reaction momentum distribution:

$$\Delta\theta = \frac{\sigma_\perp \times 2.35}{p_\parallel} \tag{8}$$

where $p_\parallel$ is the average parallel component of the ion's momentum and $\sigma_\perp$ is given by eq. 2. Since $\Delta\theta$ is determined by the production mechanism, as discussed above, and is beyond the control of the experimenter the only ways to reduce the beam emittance are to reduce x_0 or to limit the angular acceptance of the device (the latter choice lowers the secondary beam intensity, of course).

Two systems have been developed to reduce the spot size of the primary beam and improve the emittance and yield of secondary fragments. A pair of superconducting solenoidal magnets was built at GANIL to go just before and just after a high intensity target (the SISSI system) [57]. The first solenoid is used to produce a very small beam spot, approximately $x_0 \sim$0.2 mm, by acting as a strong demagnifying lens. Thus, the beam strikes the target with an angular spread that is much larger than normal. The second solenoid collects the large angular spread of the fragments. In the limit that the angular spread of the beam

was larger than the angular spread of the reaction then the resulting secondary beam emittance could be more efficiently transported to experimental areas even though the acceptance of the beam lines is quite small. A magnetic quadrupole doublet was installed just before the target position of the A1200, and later the A1900 separator, at the NSCL for similar purposes. The spot size in the former A1200 case was approximately x_0 ~1 mm and has provided about a factor of four improvement in emittance and subsequently a similar factor in transmitted beams to experiments.

4 Energy Degraders and Range Compression

Basic studies of the existence, half lives, and decay properties of the ions produced by projectile fragmentation with in-flight separation have been accomplished by slowing down and collecting them in solid materials, particularly in silicon semiconductor detectors. More detailed and important studies of fundamental properties (precise masses and isotope shifts) of nuclei produced by target fragmentation and ISOL separators use very 'slow' beams of exotic ions, e.g. after injection into precision ion traps. The ion-guide ISOL (IGISOL) technique has been used for many years to collect low energy reaction products (~1 MeV/u or so) in helium. [61] The areal thickness of the gas in these cells and thus the ability to thermalize nuclear reaction products is low but the rapid ejection of a small fraction (~percent) of very exotic nuclei has proven effective in nuclear structure studies.

It has been suggested that very fast projectile fragment beams, kinetic energy per particle~200 MeV/nucleon, can be thermalized by depositing the bulk of their energy in a solid foil and the remainder in high pressure helium gas. [62,63] The particles would remain ionized due to the high ionization potential of helium as in the IGISOL systems and could be collected with electric fields. Such a system has the potential to be a high efficiency non-selective ion source that would allow a range of new studies of exotic nuclei that are not possible at the present in-flight fragmentation facilities. This technique would require the extension of the IGISOL technology combined with an in-flight separation system. The plan for the RIA facility incorporates a high pressure gas cell for the delivery of the most exotic ions for precision studies. [19] However, there are two difficulties in just stopping the ions in a buffer gas: first, the density of a typical gas is about 1000 times lower than that of a solid causing the range distribution to be spread over large distances, second, the broad momentum distributions of ions from projectile fragment separators (several percent in most cases) will spread the large range distribution of a mononenergetic ion in gas over even larger distances.

Development projects are underway at the major fragmentation facilities around the world to collect fast ions in buffer gases (see the recent summary by Wada [64]). In these systems the fast ions lose nearly all of their kinetic energy in a degrader foil/entrance window and go into the gas cell filled with high-purity helium. These degraders have to be very carefully prepared because

imperfections in the solid on the order of a few μm turn into tens of mm in a gas. The ions will lose the remainder of their kinetic energy in the gas and will capture electrons during the final deceleration and become thermalized.

As an example of the problem of stopping a *monoenergetic* ion in a gas we can consider a monoenergetic ^{40}Ar ions at 4 GeV, i.e., 100 MeV/u. The range distribution of argon ions in solid beryllium (calculated with the Monte Carlo program SRIM-2000 program from Ziegler [66]) follows a nearly Gaussian distribution centered at 6.410 mm and has a straggling width of 24 μm. Imagine that the thickness of the beryllium foil is decreased to be just 20 μm less than the mean range and the foil is the entrance window to a chamber filled with helium at one bar. Essentially all of the ions are predicted to exit the foil and enter the helium. The range distribution of the ions in the helium can also be readily calculated and the dramaticly lower density of the gas causes the range to be long and the width to be very broad. The mean range in the gas after 6.390 mm of beryllium is calculated to be 194 mm and the width is 83.4 mm. Thus, the collection of the exotic ions that are created in nuclear reactions that occur at E/A$\sim$100 MeV/u is complicated by the effects of the integrated range straggling. The gas cell typically would have a physical size ($\sim$500 mm) and a cylindrical shape to contain the distribution of thermalized ions. In general, the high pressure gas cell needs to have an effective thickness of about 1 atmosphere-meter at room temperature (even so this corresponds to only $\sim$20mg/cm^2 of helium).

It is expected that the majority of ions will be singly charged due to the large first ionization potential of atomic helium. However, the level of primary ionization caused by the stopping process and the presence of molecular impurties in the gas play important roles and the fraction of ions that will remain ionized is controversial. The gas cell is too large for the gas and ions to be physically evacuated on a time scale that is fast enough to be useful with the most exotic ions. Thus, the ions must be drifted towards the exit hole with an electric field gradient along the length of the cell with electrodes to focus the ions at the exit hole. Various approaches to the ion sweeping are being tried at present including

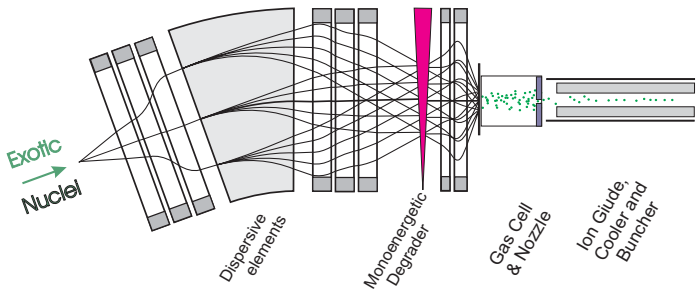

Fig. 7. The schematic representation of the range compression concept to narrow the range distribution of projectile fragments by combining a momentum dispersion with an monoenergetic wedge in front of a gas cell [62].

static and rf potentials. [67,64] Each approach has advantages and disadvantages but the discussion of ion mobility in gases goes beyond the scope of the present work.

The second problem for the efficient collection of projectile fragments is their broad momentum distribution, typically up to Δp/p=5% in modern separators, depending on the ion of interest. The combination of an ion-optical system to create a momentum dispersion at a monoenergetic wedge (as compared to the achromatic wedge described above) can be used to compress projectile-fragment range distributions. A schematic diagram of such a system is shown in Fig. 7 [62]. The angle of a thin wedge to produce a monoenergetic beam, α_M, for an ion with mass, m, and velocity, $v = \beta\gamma$, can be found from the approximate expression of Schiedenberger et al. [63]:

$$\tan(\alpha_M) \approx \frac{\gamma m \beta^2}{D(dE/dx)} \tag{9}$$

where D is the momentum dispersion of the system, dE/dx is the energy loss rate of the ion in the material, β and γ are the usual factors from relativity. A thin wedge is one in which the velocity difference of the ion between entrance and exit can be ignored. The result is that the ion beam is brought to one energy but the physical size of the beam is much greater. This large beam is then immediately sent into the gas cell, see for example Fig. 3 in Ref. [63].

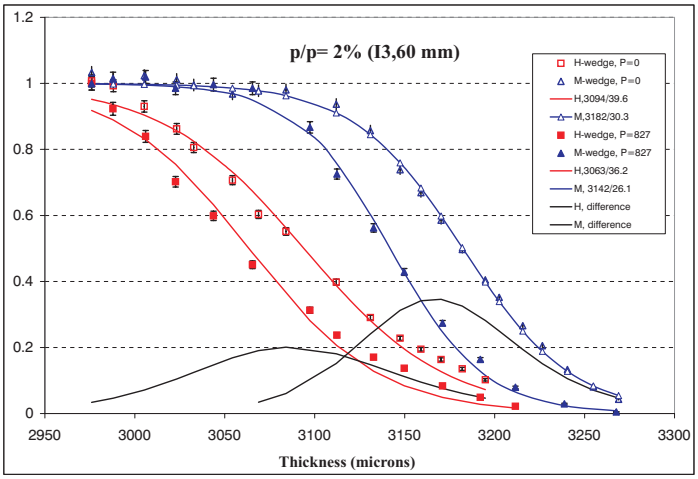

Fig. 8. The transmission curves for ^{32}P ions (Δp/p=2%) from the NSCL A1900 separator with a homogeneous degrader (square symbols) can be compared with the curves obtained with a monoenergetic wedge (triangular symbols). The open symbols are for an evacuated gas cell, the filled symbols are for helium at a pressure of 827 torr and a distance of 45 cm. The diffence between gas-in and gas-out, shown by the peaked curves, represents the fraction of ions stopped in the gas. See the text for details.

An example of range compression for ^{32}P fragments at a magnetic rigidity of Bρ=3.322±1% from an ^{40}Ar beam (140 MeV/u) is shown in Fig. 8. These measurements were obtained by Weissman et al. [65] using a system very similar to that described by Weick [62]. The secondary beam was prepared in NSCL-A1900 and dispersed onto a degrader system and a wedge. After leaving the wedge the products entered the gas cell and the residual energy was measured in a silicon semiconductor telescope. The number of transmitted ions is shown as a function of the degrader thickness combined with either a monoenergetic wedge (M, α_M=11 mrad) or a homogeneous (H,α_M ∼0 mrad) or "flat" wedge, with and without gas in the cell. The difference between the transmission curves with and without gas for a given degrader represents the fraction of ions that be stopped in the gas.

In first order, the minimum momentum spread, δ_{min}, that can be achieved in such a system is given by the expression:

$$\delta_{min} = (\frac{(x/\delta)}{(x/x)x_0})^{-1} \times (1 - \frac{t}{R})^{-1} \tag{10}$$

where x_0 is the initial beam spot size and t is the thickness in units of the range, R, of the ion. As shown by eq. 10, the quality of the momentum compression depends on the resolving power of the system, R=$\frac{(x/\delta)}{(x/x)x_0}$. The resolving power is the minimum momentum difference the system can separate. Higher order optical abberations in the system will increase the incoherent spot size, which is given in first order by $(x/x)x_0$, and limit the minimum momentum spread. Energy loss straggling will also contribute (as will non-uniformities of the degrader) and normally limit the compression to the order of 0.1%, regardless of the quality of the optical system. Similarly, the final transverse emittance, after degrading, is given by the equation:

$$\epsilon = \epsilon_0 \frac{\delta_0}{\delta} \times (1 - \frac{t}{R})^{-1} \tag{11}$$

where ϵ_0 is the initial initial emittance of the beam before the degrader and t is the thickness in units of the range, R, of the ion. Hence if the desired momentum compression if a factor of 10, the transverse emittance will grow by a factor of more than 10.

5 Summary of Existing Capabilities and Outlook

The achromatic separator technique has been implemented in several laboratories around the world that can provide a wide variety of relatively high energy primary beams. As noted in the Introduction, there are separators operating in France, Germany, Japan, and USA. The next generation of devices that use multiple stages of separation are under construction in Japan [17] or are being planned [18,19]. A comparison of the various parameters that describe the fragment separators is given in Table 2. The LISE separator has been operated for

Table 2. Comparison of Fragment Separators

device	Ω (msr)	Δp/p (%)	Bρ (T-m)	resolving power†	length (m)	reference
A1200	0.8/4.3	3.0	5.4	700/1500	22.	Sherrill 1992
A1900	8.0	5.4	6.0	∼2900	35	Morrissey 2003
COMBAS	6.4	20.	4.5	4360	14.5	Artukh 1993
LISE	1.0	5.0	3.2	800	18.	Mueller 1991
FRS	0.2	2.0	18.	1500	73.	Geissel 1992
super-FRS‡	0.8	5.0	18.	1500	∼140	Geissel 2003
RIPS	5.0	6.0	5.76	1500	21.	Kubo 1990
big-RIPS‡	8.0	6.0	9.0	1290/3300	77	Kubo 2003
RCNP	1.1	8.0	3.2	2000	14.8	Shimoda 1992

†mass-to-charge resolution, see the text
‡multistage device

more than 15 years having been upgraded several times and has provided secondary beams for a large variety of experiments. The RIPS device had the largest solid angle and momentum acceptance of operating devices, but was surpassed by the COMBAS device at the JINR at Dubna. The large horizontal acceptance of 80 cm in COMBAS is achieved by using high index dipoles. This is a novel design which has many attractive features. The A1200 and A1900(MSU), RCNP(Osaka), and FRS(GSI) separators are positioned at the beginning of the beam distribution system to allow delivery of radioactive beams to any experimental area. The FRS device at GSI has been designed for very high kinetic energies, where the fragmentation cone and relative energy spread are smaller and therefore allow the physical acceptance of the device to be smaller. The next generation of devices will use multiple stages of separation to provide high acceptances and pure secondary beams. The new devices will use superconducting magnets, this technology was pioneered with the NSCL A1200 separator and refined for the A1900 separator.

References

1. Y.P. Viyogi et al., Phys. Rev. Lett. **42**, 33 (1979).
2. J. Alonso, A. Chatterjee, and C.A. Tobias, 1978, IEEE Trans. on Nucl. Sci. **NS-26**, 3003 (1978).
3. Proc. of the Workshop on Research with Radioactive Beams, Washington DC, Lawrence Berkeley Laboratory Report LBL-18187, unpublished, (1984).
4. J.P. Dufour et al., Nucl. Instr. and Meth. **A 248**, 267 (1986).
5. R. Anne et al., Nucl. Instr. and Meth. **A 257**, 215 (1987).
6. K.-H. Schmidt et al., Nucl. Instr. and Meth. **A 260**, 287 (1987).
7. H. Geissel et al., Nucl. Instr. and Meth. **A 282**, 247 (1989).
8. B. Blank et al. Phy. Rev. Lett., **84**, 1116 (2000).
9. R. Schneider et al., Z. Phys. **A 348**, 241 (1994).
10. M. Lewitowicz et al. Phys. Lett. **B 322**, 20 (1994).

11. B.M. Sherrill et al., Nucl. Instr. and Meth. **B 70**, 298 (1992).
12. T. Kubo et al., In *Proc. First Intl. Conf. on Radioactive Nuclear Beams*, W.D. Myers, J.M. Nitschke, and E. Norman, eds. (World Scientific, Singapore, 1990) pp. 563-572.
13. H. Geissel et al., Nucl. Inst. and Meth. **B 70**, 286 (1992).
14. A.G. Artukh et al., In *Proc. Third Intl. Conf. on Radioactive Nuclear Beams*, D.J. Morrissey, ed. (Editions Frontieres, Gif-sur-Yvette, 1993) pp. 45-48.
15. A.C. Mueller, and R. Anne, Nucl. Instr. and Meth. **B 56/57**, 559 (1991).
16. D.J. Morrissey et al., Nucl. Instr. and Meth. **B 204**, 90 (2003), and references therein.
17. T. Kubo et al., Nucl. Instr. amd Meth. **B 204**, 97 (2003), and references therein.
18. H. Geissel et al., Nucl. Instr. and Meth. **B 204**, 71 (2003), and references therein.
19. B.M. Sherrill, Nucl. Instr. and Meth. **B 204**, 765 (2003), and RIA Task Force Report, (1999), http://srfsrv.jlab.org/isol/ISOLTaskForceReport.doc
20. J.A. Nolen, and L. Harwood, Instrumentation for Heavy Ion Nuclear Research, D. Shapira, ed. (Harwood, New York, 1985) 171.
21. K. Sümmerer and B. Blank, Phys. Rev. **C 61**, 034607 (2000).
22. B.M. Sherrill, In *Proc. Intl. Conf. on Radioactive Nuclear Beams*, Th. Delbar, ed. (Adam Hilger, London, 1992) pp. 1-20.
23. G. Münzenberg, Nucl. Instr. and Meth. **B 70**, 265 (1992).
24. H. Geissel, G. Münzenberg, and K. Riisager, Ann. Rev. Nucl. Part. Sci. **45**, 163 (1995).
25. D.J. Morrissey and B.M. Sherrill, Phil. Trans. R. Soc. London **A**356, 1985 (1998).
26. C.N. Davids, and J.D. Larson, Nucl. Instr. and Meth. **B 40/B41**, 1224 (1989).
27. R.E. Tribble, R.H. Burch, and C.A. Gagliardi, Nucl. Instr. and Meth. **A 285**, 441 (1989).
28. H. Wollnik, Optics of Charged Particles, (Academic Press:Boston, 1989).
29. M. Bernas et al., Phys. Lett. **B 331**, 19 (1994).
30. K.E. Rehm et al., Nucl. Instr. and Meth. **A 370**, 438 (1996).
31. A.S. Goldhaber and H.H. Heckmann, Ann. Rev. Nucl. Part. Sci. **28**, 161 (1978).
32. J. Hüfner, Phys. Rep. **125**, 129 (1985).
33. D.J. Morrissey et al., Phys. Rev. Lett. **43**, 1139 (1979).
34. Y. Yariv and Z. Fraenkel, Phys. Rev. **C 20**, 2227 (1979).
35. Y. Yariv and Z. Fraenkel, Phys. Rev. **C 24**, 488 (1981).
36. M. Fauerbach, Diplomarbeit, T.H. Darmstadt, 1992.
37. J.D. Bowman, W.J. Swiatecki, and C.F. Tsang, Lawrence Berkeley Laboratory Report, LBL-2908, (1973), unpublished.
38. J. Gosset et al., Phys. Rev. **C 16**, 629 (1977).
39. D.J. Morrissey et al., Phys. Rev. **C 18**, 1267 (1978).
40. J.-J. Gaimard and K.-H. Schmidt, Nucl. Phys. **A 531**, 709 (1991).
41. M. deJong, A.V. Ignatyuk, K.-H. Schmidt, Nucl. Phys. **A 613**, 435 (1997).
42. G.A. Souliotis et al., Phys. Lett. **B 543**, 163 (2002).
43. T. Enqvist et al., Nucl. Phys. **A 703**, 435 (2002).
44. K. Sümmerer and D.J. Morrissey, In *Proc. First Intl. Conf. on Radioactive Nuclear Beams*, W.D. Myers, J.M. Nitschke, and E. Norman, eds. (World Scientific, Singapore, 1990) pp. 122-131, and K. Sümmerer et al., Phys. Rev. **C 42**, 2546 (1990).
45. G. Rudstam, Z. Naturforsch. **21a**, 1027 (1966).
46. G.A. Souliotis et al., Phys. Rev. **C 46**, 1383 (1992).
47. R. Pfaff et al., Phys. Rev. **C 53**, 1753 (1996).

48. A.S. Goldhaber, Phys. Lett. **B 53**, 306 (1974).
49. G. Bertsch, Phys. Rev. Lett. **46**, 472 (1981).
50. D.J. Morrissey, Phys. Rev. **C 39**, 406 (1989).
51. K. Van Bibber et al., Phys. Rev. Lett. **43**, 840 (1979).
52. R. Pfaff et al., Phys. Rev. **C 51**, 1348 (1995).
53. K. Asahi et al., Phys. Lett. **251B**, 488 (1990).
54. H. Okuno et al., Phys. Lett. **335B**, 29 (1994).
55. D. Groh et al., Phys. Rev. Lett. **90**, 202502 (2003).
56. K.-H. Schmidt et al., Nucl. Phys. **A 701**, 115 (2002), and references therein.
57. A. Savalle et al., In *Proc. EPAC96 Fifth European Particle Accelerator Conf.*, (IoP Publishing, 1996) pp. 2403-2405, and A. Joubert et al., GANIL Report A-91-01, (1991) unpublished.
58. J.A. Nolen et al., Nucl. Instr. and Meth. **B 204**, 293 (2003), ibid. pp. 298-302.
59. O.B. Tarasov and D. Bazin, Nucl. Instr. and Meth. **B 204**, 174 (2003), and references therein.
60. N. Iwasa, H. Geissel, G. Münzenberg, C. Scheidenberger, Th. Schwab, H. Wollnik, Nucl. Instr. and Meth. **B 126**, 284 (1997).
61. P. Dendooven, Nucl. Instrum. Meth. **B126**, 182 (1997), and references therein.
62. H. Weick et al., Nucl. Instrum. Meth. **B 164-165**, 168 (2000).
63. C. Scheidenberger et al., Nucl. Instr. and Meth. **B 204**, 119 (2003).
64. M. Wada et al., Nucl. Instr. and Meth. **B 204**, 570 (2003).
65. L. Weissman et al., Nucl. Instr. and Meth. (2003) submitted for publication.
66. J.F. Ziegler, "The Stopping and Range of Ions in Matter (SRIM-2000)", http://www.research.ibm.com/ionbeams/#SRIM
67. G. Savard et al., Nucl. Instr. and Meth. **B 204**, 582 (2003).